Inorganic Chemistry

pubs.acs.org/IC

Article

Rapid Thermodynamically Stable Complex Formation of [nat/111In]In3+, [nat/90Y]Y3+, and [nat/177Lu]Lu3+ with H6dappa

Thomas I. Kostelnik, Xiaozhu Wang, Lily Southcott, Hannah K. Wagner, Manja Kubeil, Holger Stephan, María de Guadalupe Jaraquemada-Peláez,* and Chris Orvig*

Cite This: https://dx.doi.org/10.1021/acs.inorgchem.0c00671

Read Online

ACCESS | Metrics & More | Article Recommendations | Supporting Information

ABSTRACT: A phosphinate-bearing picolinic acid-based chelating ligand (H_6dappa) was synthesized and characterized to assess its potential as a bifunctional chelator (BFC) for inorganic radiopharmaceuticals. Nuclear magnetic resonance (NMR) spectroscopy was employed to investigate the chelator coordination chemistry with a variety of nonradioactive trivalent metal ions (In^{3+}, Lu^{3+}, Y^{3+}, Sc^{3+}, La^{3+}, Bi^{3+}). Density functional theory (DFT) calculations explored the coordination environments of aforementioned metal complexes. The thermodynamic stability of H_6dappa with four metal ions (In^{3+}, Lu^{3+}, Y^{3+}, Sc^{3+}) was deeply investigated via potentiometric and spectrophotometric (UV−vis) titrations, employing a combination of acidic in-batch, joint potentiometric/spectrophotometric, and ligand−ligand competition titrations; high stability constants and pM values were calculated for all four metal complexes. Radiolabeling conditions for three clinically relevant radiometal ions were optimized ([111In]In^{3+}, [177Lu]Lu^{3+}, [90Y]Y^{3+}), and the serum stability of $[^{111}In][In(dappa)]^{3-}$ was studied. Through concentration-, time-, temperature-, and pH-dependent labeling experiments, it was determined that H_6dappa radiolabels most effectively at near-physiological pH for all radiometal ions. Furthermore, very rapid radiolabeling at ambient temperature was observed, as maximal radiolabeling was achieved in less than 1 min. Molar activities of 29.8 GBq/μmol and 28.2 GBq/μmol were achieved for [111In]In^{3+} and [177Lu]Lu^{3+}, respectively. For H_6dappa, high thermodynamic stability did not correlate with kinetic inertness—lability was observed in serum stability studies, suggesting that its metal complexes might not be suitable as a BFC in radiopharmaceuticals.

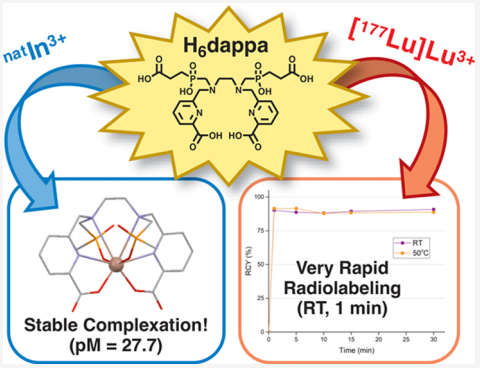

INTRODUCTION

Radiopharmaceuticals are drugs that rely on the physical decay of a radionuclide to elicit a diagnostic or therapeutic response. While "organically-derived" radiotracers, which employ non-metal radionuclides (e.g., ^{18}F, ^{11}C, ^{123}I), have received considerable attention in the field of nuclear medicine, metal-based radiopharmaceuticals are undoubtedly more versatile and hold great promise, particularly with respect to therapeutics.[1] Their protean nature is owed to the range of radionuclides that span main-group, transition, and *f*-block metals and afford a wide-variety of decay types/energies, half-lives, and chemical properties. For example, [111In]In^{3+} ($t_{1/2}$ = 67.2 h) is a clinically used single-photon emission computed tomography (SPECT) imaging radionuclide due to its low energy γ-emission (Eγ = 171 and 245 keV; Iγ = 91 and 94%, respectively) following electron capture, which has led to its inclusion in a number of clinically approved radiotracer agents.[1,2] Alternatively, [177Lu]Lu^{3+} ($t_{1/2}$ = 159 h) is a therapeutic radionuclide due to its low-energy β^- emission ($E\beta^-_{avg}$ = 134 keV, 100%), which has been proven to exert a significant therapeutic effect and recently received FDA approval for the treatment of somatostatin receptor-positive gastroenteropancreatic neuroendocrine tumors under the brand name Lutathera ([177Lu][Lu-DOTA-TATE]).[3,4] The differences between these two radiometals alone exemplify the variety of decay characteristics available across the Periodic Table (or more specifically the Chart of Radionuclides[5]), which permit inorganic radiochemists to harness an exceptionally broad range of properties during the drug discovery process. When paired with the increasingly powerful technology surrounding *in vivo* targeting, inorganic nuclear medicine has become an exciting field of research with an abundance of potential.

The multitude of choice associated with inorganic radionuclides is accompanied by a caveat: to ensure the selected radiometal ion accumulates at the desired tissues *in vivo*, bioconjugates are commonly required to serve as targeting vehicles. Direct radiolabeling of these biological molecules is a rarity; rather bioconjugates are typically modified with

Received: March 3, 2020

Chart 1. Chemical Structures of Selected Chelators

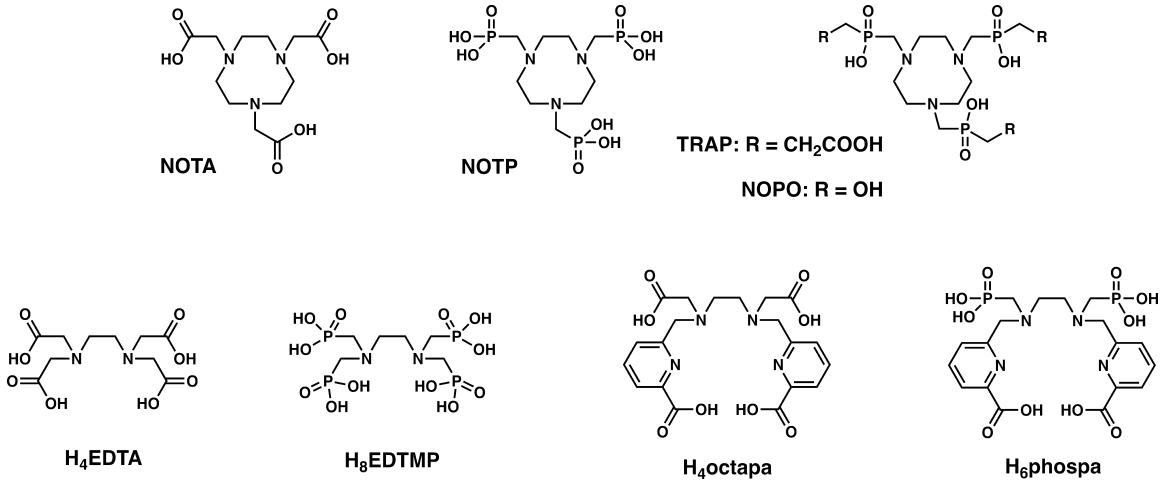

Scheme 1. Design Principal of H_6dappa

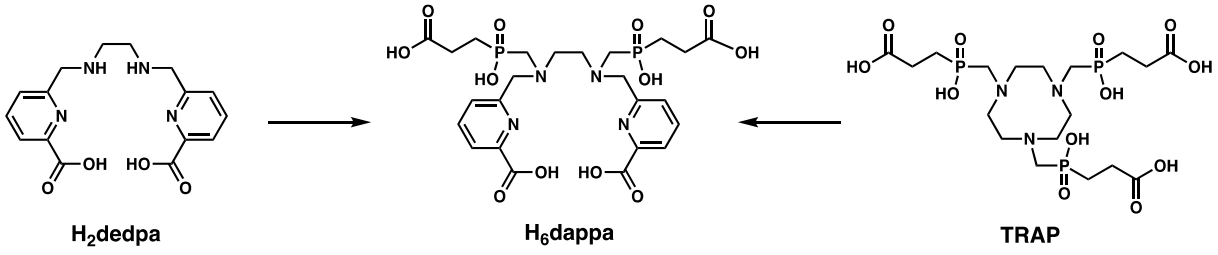

bifunctional chelating ligands (BFCs), which securely coordinate and hold radiometal ions, and also provide a handle for covalent linkage with a bioconjugate. While the latter is typically achieved through only a handful of common strategies (e.g., amide, thiourea, maleimide, and 1,2,3-triazole linkages),[6,7] radiometal ion chelation is a complex and diverse topic, requiring detailed knowledge of fundamental coordination chemistry to properly match chelators to radiometals[8] and achieve optimal drug performance. As the diversity of chemical and physical properties across metal ions precludes a one-size-fits-all chelator, continued research in the field of chelator development is crucial to discover chelating ligands capable of forming thermodynamically stable and kinetically inert complexes with each radiometal of interest.

The investigation of phosphonate-containing chelators has seen continued interest over recent years (Chart 1), in part due to the versatility of their coordination chemistry and biological applications. In general, phosphonates are known for their rapid exchange kinetics and "hard" coordinating properties (denoting ionic-dominated interactions with metals).[9] Expectedly, phosphonate incorporation in chelators designed for hard metals (e.g., $[^{67/68}Ga]Ga^{3+}$, $[^{153}Sm]Sm^{3+}$, $[^{177}Lu]Lu^{3+}$) has yielded very encouraging results, notably at the clinical level.[10−13] Also intriguing are examples of "borderline-soft" metal ions (e.g., $[^{64}Cu]Cu^{2+}$, $[^{111}In]In^{3+}$, $[^{213}Bi]Bi^{3+}$) forming stable complexes with phosphonate-containing chelators.[14−16]

The biological role of phosphonates on BFCs is also quite multifaceted. Naturally, the high affinity of (bis)phosphonates toward hydroxyapatite (HA—the mineral matrix that makes up cortical bone)[17] has led to extensive use as bone targeting agents, most notably in $[^{153}Sm][Sm(EDTMP)]^{5-}$ (Quadramet) and $[^{177}Lu][Lu(EDTMP)]^{5-}$ for bone pain palliation.[12,18] Nontargeting (purely coordinating) phosphonate-containing BFCs with *in vivo* behavior dictated by bioconjugates also exist in the literature,[14,19,20] albeit to a much lesser extent. This is likely due to difficulties controlling the inherent affinity of (bis)phosphonates toward bone; this issue appears to be mitigated through the use of phosphinates, which are similarly "hard" and present a low kinetic barrier for coordination but scantily adsorb to HA.[21] The most recognizable examples of this alteration in nuclear medicine come from variation of the phosphonate-containing [9]aneN$_3$, NOTP,[22,23] to phosphinate-containing derivates, TRAP[24−27] and NOPO.[28,29] Not only does this modification lessen the likelihood of bone accumulation (of $[^{68}Ga]Ga^{3+}$), but it also presents a site for bioconjugation.

In 2014, our group reported H_6phospa-trastuzumab, an acyclic picolinic acid-based chelating ligand containing two pendant phosphonate groups for radiometal ion coordination, conjugated to a common *HER2*-targeting monoclonal antibody.[15] While high molar activity with $[^{111}In]In^{3+}$ and $[^{177}Lu]Lu^{3+}$ was achieved, bone accumulation *in vivo* was a clear sign of poor complex kinetic inertness. It was our hypothesis that the conversion of the phosphonates to phosphinates would mitigate bone accumulation, as well as present an interesting alternative to *p*-SCN-Bn bifunctionalization of our family of picolinic acid (pa) chelators (Scheme 1).

Herein, we report the bifunctional chelator, H_6dappa, as a phosphinate-containing octadentate chelator for the high coordination number radiometal ions $[^{90}Y]Y^{3+}$, $[^{111}In]In^{3+}$, and $[^{177}Lu]Lu^{3+}$; we describe the synthesis, nonradioactive metal complexation, solution studies, radiolabeling, and structural analysis *via* density functional theory (DFT) calculation of H_6dappa.

https://dx.doi.org/10.1021/acs.inorgchem.0c00671
Inorg. Chem. XXXX, XXX, XXX−XXX

Scheme 2. Synthetic Scheme for H_6dappa

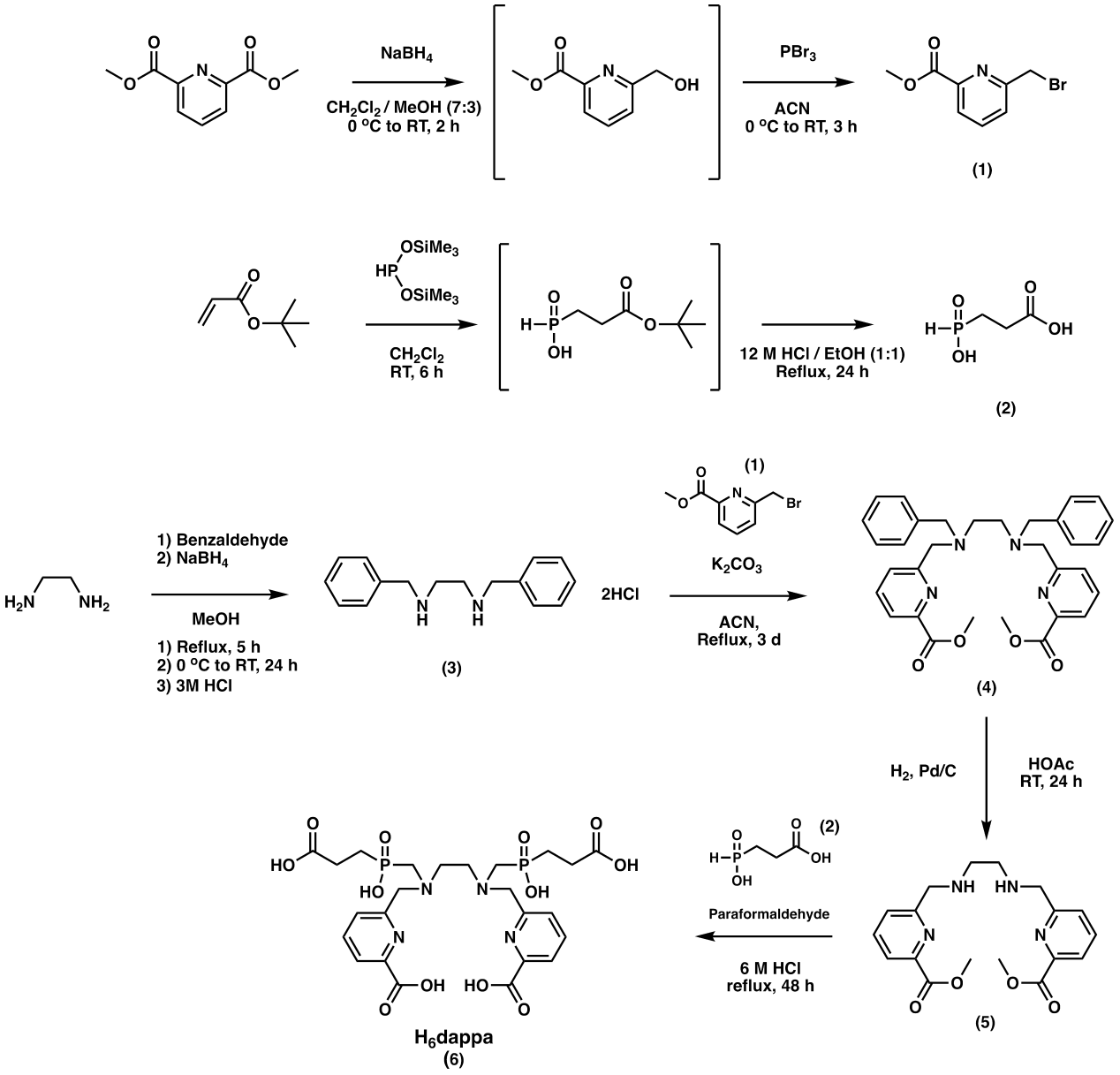

RESULTS AND DISCUSSION

Ligand Synthesis and Characterization. The strategy for the synthesis of H_6dappa (6,9-bis[{6-carboxypyridin-2-yl}methyl]-4,11-dihydroxy-4,11-dioxo-6,9-diaza-4λ^5,11λ^5-diphosphatetradecanedioic acid) was to separately synthesize each pair of coordinating arm groups (compounds **1** and **2**) and then add them stepwise to ethylene diamine following benzyl protection/deprotection (Scheme 2). The synthesis of compound **1** (methyl-6-bromomethylpicolinate) was achieved through the asymmetric reduction of dimethyl pyridine-2,6-dicarboxylate with $NaBH_4$, resulting in an alcohol primed for halogenation. PBr_3 is a very effective reagent for this purpose, especially considering the highly electron-poor nature of the methylene bridge. Although previous reports from us[30] and others[31,32] have purified the alcohol prior to bromination, this was found to be unnecessary, as the dimethyl pyridine-2,6-dicarboxylate starting material undergoes no change in the following reaction and is removed during column purification, and the over-reduced product (pyridine-2,6-diyldimethanol) is twice brominated to 2,6-bis(bromomethyl)pyridine and is separated from the desired product using hexane and ethyl acetate as eluents during column purification. These reactions are scalable (~10 g) and extremely reliable. Compound **2** is slightly more challenging to synthesize due to the pyrophoric nature of bis(trimethylsilyl) phosphonite and the time-dependent nature of the Michael-type addition. Fortunately, with careful monitoring, neither step requires purification and both are high yielding. These reactions are also easily scalable (~10−40 g)—for a detailed description see Notni et al.[33] Reductive alkylation of ethylene diamine with benzaldehyde and sodium borohydride was high yielding and conveniently purified, as 3 M HCl was used to salt-out the desired product as a dihydrochloride salt. Conveniently, following quenching of the reaction and evaporation of solvent, simple precipitation, filtration, and washing yield pure product. Again, this reaction is very reliable and easy, ultimately yielding three components (compounds **1**, **2**, and **3**) that can be produced in large

https://dx.doi.org/10.1021/acs.inorgchem.0c00671
Inorg. Chem. XXXX, XXX, XXX−XXX

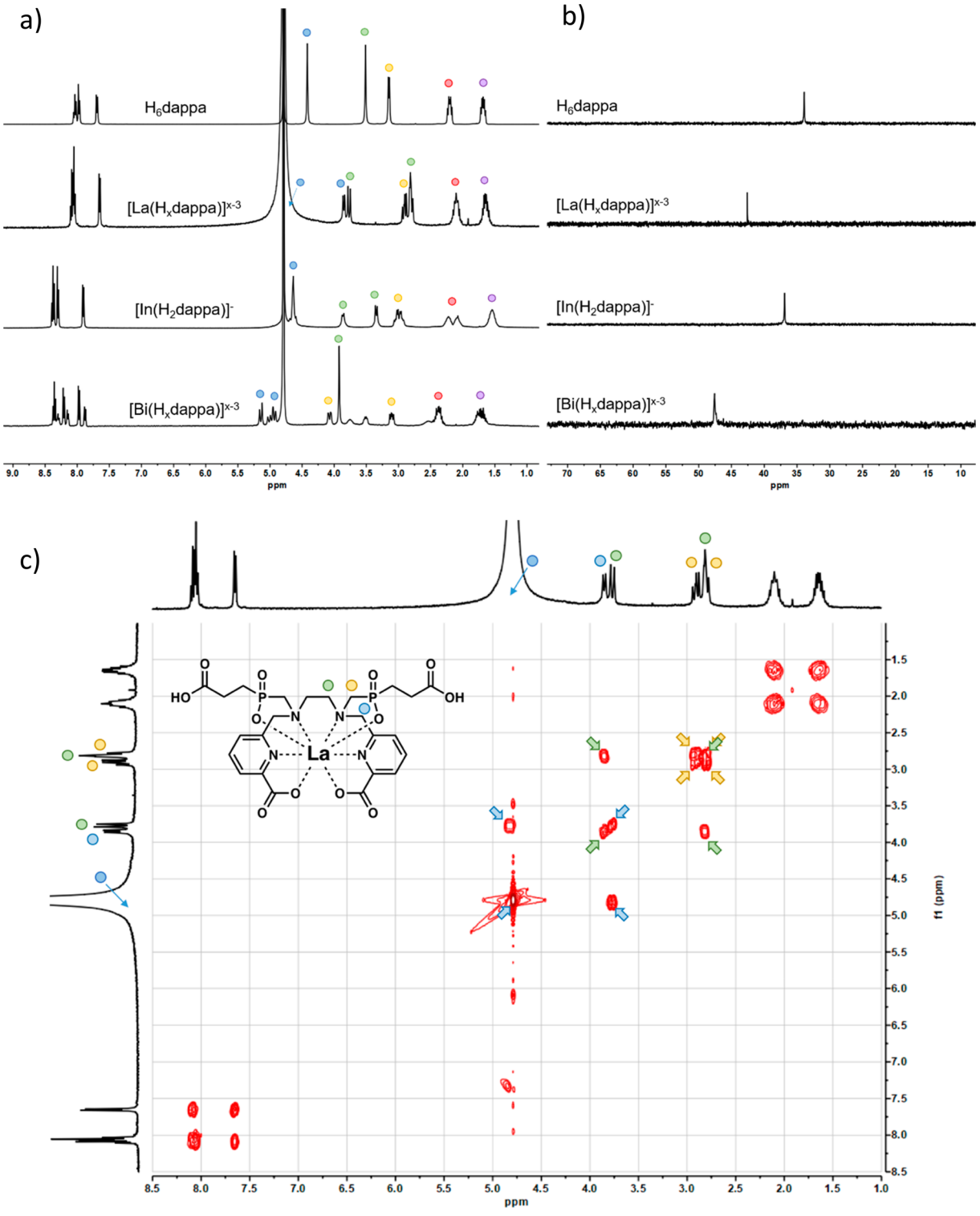

Figure 1. (a) ^{1}H NMR spectra of H_6dappa, $[La(H_x dappa)]^{x-3}$, $[In(H_2 dappa)]^{-}$, and $[Bi(H_x dappa)]^{x-3}$ (top to bottom) (D_2O, 400 MHz, 298 K). (b) $^{31}P\{^{1}H\}$ NMR spectra of H_6dappa, $[La(H_x dappa)]^{x-3}$, $[In(H_2 dappa)]^{-}$, and $[Bi(H_x dappa)]^{x-3}$ (top to bottom) (D_2O, 162 MHz, 298 K). (c) $^{1}H-^{1}H$ COSY-45 NMR spectrum of $[La(H_x dappa)]^{x-3}$ (x = not determined). Ligand/La^{3+} spectra pD 7, In^{3+}/Bi^{3+} spectra pD 1.

quantities in preparation for the following three reactions (Scheme 2).

Compound **4** is produced through an S_N2 reaction wherein each of the secondary amines of **3** attacks the bromomethylene bridge of **1**. A large excess (~7 equiv) of K_2CO_3 is used to neutralize the 2 equiv of HCl from **3** and maintain a very basic environment to facilitate amine deprotonation. Liquid−liquid (DCM/H_2O) extraction and purification via silica column chromatography with hexane and ethyl acetate led to a moderate yield (57%) on a sufficiently large scale (~1.5−2.0 g). Compound **5** is produced by deprotection of benzyl groups via palladium on carbon (Pd/C) hydrogenation. This straightforward procedure is achieved at ambient temperature and does not require further purification following filtration (to

https://dx.doi.org/10.1021/acs.inorgchem.0c00671
Inorg. Chem. XXXX, XXX, XXX−XXX

remove Pd/C) and evaporation of solvent. The final ligand (H_6dappa; **6**) is prepared via tandem acid-mediated methyl ester hydrolysis and Kabachnik–Fields reaction, where **5** and an excess of **2** (4 equiv) are dissolved in refluxing 6 M HCl and a large excess of paraformaldehyde (15 equiv) added over 48 h. A challenging aspect of this final step is the removal of the excess **2** and presumed side-product (3-[hydroxyl-{hydroxymethyl}phosphoryl]propanoic acid) due to their similar retention on our HPLC column (Phenomenex Synergi 4 μm hydro-RP 80 Å), which led to inefficient and time-consuming separation. Instead, crude purification by cation-exchange chromatography (DOWEX 50WX2, H^+ form) easily separated the amine-containing H_6dappa from neutral and anionic impurities. Following concentration of the semipure eluate, HPLC purification (Figure S8) and lyophilization yielded pure H_6dappa as a fluffy white solid.

Metal Complexation. Complexation was studied with the nonradioactive metal ions In^{3+}, Y^{3+}, Lu^{3+}, and Sc^{3+} due to our interest in eventual study of their radioisotope counterparts (i.e., $[^{111}In]In^{3+}$, $[^{86/90}Y]Y^{3+}$, $[^{177}Lu]Lu^{3+}$, and $[^{44/47}Sc]Sc^{3+}$). Additional experiments were conducted with Bi^{3+} and La^{3+} to gain further understanding of H_6dappa coordination chemistry.

Characterization was confirmed by $^1H/^{31}P\{^1H\}$ NMR spectroscopy and high-resolution electrospray ionization mass spectrometry (HR-ESI-MS), as well as $^1H-^1H$ correlated spectroscopy (COSY) and $^1H\{^{31}P\}$ NMR when appropriate. A characteristic sign of metal complex formation is diastereotopic splitting of methylene protons that are equivalent in the ^1H NMR spectra of the free ligand. This phenomenon is observed with each of the studied metal ions, with varying degrees of spectral complexity and fluxionality. For example, the $[In(H_2dappa)]^-$ ^1H NMR spectrum reveals relatively sharp peaks, with protons on the ethylene backbone, an amine-methylene-phosphinate bridge, and protons adjacent to the terminal aliphatic carboxylic acids exhibiting diastereotopic splitting. Cross-peaks in the $^1H-^1H$ COSY spectrum (Figure S11) confirmed our interpretation. The downfield shift in the $^{31}P\{^1H\}$ NMR spectra also confirms the coordination of the phosphinate group. The simplicity of all $[In(H_2dappa)]^-$ NMR spectra suggests a rigid symmetric complex (In^{3+} ionic radius = 0.92 Å, CN = 8).[34] Spectra of the yttrium(III), lutetium(III), and scandium(III) complexes are increasingly complicated. Complexation of Y^{3+}, the largest of the three rare-earth metals (ionic radius = 1.02 Å, CN = 8),[34] results in a moderately convoluted ^1H NMR spectrum; however, identification of major and minor isomers was possible by analyzing the aromatic protons with $^1H-^1H$ COSY (Figure S14). More complicated were the spectra of Lu^{3+} (ionic radius = 0.98 Å, CN = 8)[34] and Sc^{3+} (ionic radius = 0.87 Å, CN = 8);[34] the $^{31}P\{^1H\}$ NMR spectra of both complexes reveal the presence of multiple isomers, which can also be noted in the aromatic region of the ^1H NMR spectra. The complicated nature of these spectra made it difficult to draw conclusions beyond confirming complexation.

To further investigate the relationship between metal ion size and spectral complexity, two additional metal ions were studied—La^{3+} (ionic radius = 1.16 Å, CN = 8)[34] and Bi^{3+} (ionic radius = 1.17 Å, CN = 8).[34] As seen in Figure 1a, the La^{3+} complex behaved as expected, with the ^1H NMR spectrum displaying sharp peaks with characteristic diastereotopic splitting, indicative of a highly rigid and symmetrical structure. $^1H-^1H$ COSY and $^1H\{^{31}P\}$ experiments (Figure 1c and Figure S20, respectively) confirmed peak assignments. The ^1H NMR spectrum of the Bi^{3+} complex was also easily interpreted and clearly representative of a symmetrical coordination complex, albeit with a minor isomer present.

Solution Thermodynamics of H_6dappa. Before interactions of new chelators with metal ions can be probed, the ligand itself must first be studied to quantify the acidity of ionizable protons, as they play a competitive role in the complex formation equilibria with metal ions. Combined potentiometric–spectrophotometric titrations were performed to determine protonation constants of H_6dappa between pH 2–11.5. Due to electrode limitations below pH 2, potentiometric titrations were not possible; acidic in-batch UV titrations were conducted to determine the most acidic pK_a values. In theory, there are ten H_6dappa pK_a values to be observed; however, determination of the most acidic proton dissociation with standard methods proved ineffective. Table 1 contains the calculated protonation constants of H_6dappa; HypSpec2014[35] and Hyperquad2013[36] programs were used to fit spectrophotometric and potentiometric titration data, respectively.

Table 1. Protonation Constants of H_6dappa

Equilibrium Reaction	log β	log K
$L^{6-} + H^+ \leftrightarrows HL^{5-}$	7.96(1)	7.96(1)[a]
$HL^{5-} + H^+ \leftrightarrows H_2L^{4-}$	13.44(2)	5.48(2)[a]
$H_2L^{4-} + H^+ \leftrightarrows H_3L^{3-}$	18.07(2)	4.63(2)[a]
$H_3L^{3-} + H^+ \leftrightarrows H_4L^{2-}$	22.20(2)	4.13(2)[a]
$H_4L^{2-} + H^+ \leftrightarrows H_5L^-$	24.91(3)	2.71(3)[a]
$H_5L^- + H^+ \leftrightarrows H_6L$	27.33(2)	2.42(2)[a]
$H_6L + H^+ \leftrightarrows H_7L^+$	29.00(2)	1.67(2)[b]
$H_7L^+ + H^+ \leftrightarrows H_8L^{2+}$	30.00(1)	1.00(1)[b]
$H_8L^{2+} + H^+ \leftrightarrows H_9L^{3+}$	29.89(1)	−0.11(1)[b,c]

[a]From potentiometric and spectrophotometric titrations, I = 0.16 M (NaCl) and 298 K. [b]From in-batch UV spectrophotometric titrations, I = 0.16 M (NaCl) and 298 K. [c]At 298 K, not evaluated at constant ionic strength.

The first deprotonation observed was at pH −0.11(1) and is attributed to a pyridine proton. This assignment is based on precedent from similar compounds[30,37,38] and the decrease in UV absorbance upon deprotonation of the picolinate chromophore (Figure S25). We hypothesize that the other pyridine deprotonates below pH −0.11(1). The next two deprotonation events occur at pH 1.00(1) and 1.67(2) and are attributed to the phosphinate groups, both because of the theoretical acidity of phosphinates versus other ionizable protons on H_6dappa, as well as the agreement of the less acidic phosphinate's pK_a with that reported for TRAP.[33] Next, the remaining four acid groups deprotonate in their expected pH ranges—the picolinic acids at 2.42(2) and 2.71(3), followed by the aliphatic carboxylic acids at 4.13(2) and 4.63(2). These values also closely match similar "pa" based ligands[30,37] and TRAP,[33] respectively. The remaining deprotonation events must then be a result of amine deprotonation at pH 5.48(2) and 7.96(1). Figure S26 illustrates the speciation with respect to pH of H_6dappa and was calculated using HySS software.[39] Interestingly, due to the multitude of ionizable protons, at any given pH < 8, three or more species exist in solution.

Complex Formation Equilibria of H_6dappa with In^{3+}, Lu^{3+}, Sc^{3+}, and Y^{3+}. The formation of thermodynamically stable metal complexes is a requirement of a good chelator. While the degree of required or desired complex stability varies

https://dx.doi.org/10.1021/acs.inorgchem.0c00671
Inorg. Chem. XXXX, XXX, XXX–XXX

across applications (*e.g.*, chelation therapy, treatment of bone disorders, metal chaperones), for tumor-targeting radiopharmaceuticals (excluding bone metastases), typically the goal is to achieve as stable a complex as possible. Stability is commonly conveyed in terms of formation constants (log K_{MpHrLq}), which convey the thermodynamic drive for complex formation through the sum of numerous equilibrium equations and are conventionally expressed and compared in terms of metal ion (M) and ligand (L) association ($pM^{3+} + qL^{z-} + rH^{+} \leftrightarrow MpHrLq^{3p+r-qz}$). It should be noted that protons (H^{+}) also play a role in this equilibrium, as they compete with metals for occupation of coordinating electron pairs of ligands (chelators). pM values ($pM = -\log[M_{free}]$) are another useful thermodynamic parameter that expresses the metal sequestering ability of a ligand in terms of free metal ion concentration under standard conditions ([L] = 10 μM, [M] = 1 μM, pH 7.4).[40] The power of pM values is the ability to more justifiably compare them across different ligands, protonation states, denticities, and metal ions, as well as their linear correlation with stability constants. In both cases, high values indicate high thermodynamic stability.

Complex formation equilibria studies with H_6dappa were carried out with stable natural isotopes of In^{3+}, Lu^{3+}, Sc^{3+}, and Y^{3+} (due to the concomitant availability of attractive radioisotopes) with several methods to ensure data completeness and result validation. Direct potentiometric−spectrophotometric titrations were used to detect MH_xL (x = 3, 2, 1, 0, −1) deprotonation events and ligand−ligand competition titrations (with H_6TTHA or H_4EDTA; Tables S3 and S4) used to substantiate these values. In each case, metal complexes formed below pH 2, likely as a result of deprotonated phosphinate groups maintaining high affinity for free metal ions as low as pH 0. Thus, acidic in-batch UV spectrophotometric titrations were necessary to monitor complex formation, and were achieved by taking advantage of differences between ligand and metal−ligand complex UV absorbance profiles (Figures S27−S31). Iterative fitting was performed using HypSpec2014[35] and Hyperquad2013[36] to ensure accuracy of calculated values; stability constants are presented in Table 2. Speciation plots were calculated using HySS software[39] and are presented in Figure 2.

H_6dappa forms highly stable complexes with In^{3+}, Lu^{3+}, Sc^{3+}, and Y^{3+} as evidenced by the high stability constants and pM values (Figure 3). Of particular interest is the impressive pIn value (27.7), which is greater than that for either widely used and commercially available chelators DOTA (1,4,7,10-tetracyclododecane-1,4,7,10-tetraacetic acid; 18.8) or DTPA (1,1,4,7,7,-diethylenetriaminepentaacetic acid; 25.7), as well as other strongly performing chelators such as H_4octapa[30] (26.5), H_4neunpa[41] (23.6), and H_4octox[42] (25.0) (Table S5). The pLu value (18.6) is also notable; it exceeds that of DOTA[43] (17.1) and H_4octox[42] (18.2) and is comparable to that of DTPA[43] (19.1) or H_4octapa[43] (19.8). The speciation diagrams illustrate the one species present at physiological pH for each metal complex—a desirable characteristic as multiple species can present challenges throughout additional studies, most notably *in vivo*. Ultimately, these encouraging results led to further experiments probing the ability of H_6dappa to serve as a bifunctional chelator for radiopharmaceutically relevant metal ions.

Preliminary Radiolabeling and Human Serum Challenge Experiments. The mark of a promising chelator is the ability to achieve high molar activity (i.e., high radiochemical yield [RCY] at low ligand concentration) and for the complex to remain kinetically inert when challenged with extraneous ligands or metal ions. Our preliminary radiolabeling experiments explore the highest possible molar activity achievable with H_6dappa using a variety of clinically relevant radionuclides. This goal was achieved through concentration-, time-, temperature-, and pH-dependent radiolabeling experiments, all of which were monitored by radio-TLC (thin-layer chromatography). The mobile phase used was a mixture of NH_4OH/MeOH/H_2O (1/10/20), which has been used to study RCY with a number of other phosphonate-bearing chelators.[44−47] HPLC was initially pursued as a method of RCY determination; however, the high hydrophilicity of $[M(H_xdappa)]^{3-x}$ (x = 1, 2) prevented the differentiation of free radiometal ions and complexes due to elution of both radiometal species at the solvent front (Figure S32). It was noted that the difference in peak shape between free $[^{111}In]In^{3+}$ and labeled activity using an isocratic HPLC gradient (broad vs sharp) did qualitatively suggest successful radiolabeling.

Given the promising thermodynamic results with Y^{3+}, In^{3+}, and Lu^{3+} (*vide supra*) optimizing the RCYs with $[^{90}Y]Y^{3+}$, $[^{111}In]In^{3+}$, and $[^{177}Lu]Lu^{3+}$ was the focus. Typically, "pa" family ligands are radiolabeled at pH 4;[30,41,48,49] thus, our first radiochemical studies with $[^{177}Lu]Lu^{3+}$ were conducted at pH 2, 4, 5.5, and 7. Labeling reactions were spotted on TLC plates at 1, 5, 10, 15, and 30 min to study radiolabeling kinetics. Ligand concentrations were also varied stepwise, decreasing by a factor of 10 from 10^{-4} M until 10^{-7} M. Reactions were also done at ambient temperature and at 50 °C to study the effect of heating on RCY and labeling kinetics. Several trends can be noted from the preliminary results presented in Table S6. Clearly, radiolabeling H_6dappa with $[^{177}Lu]Lu^{3+}$ at higher pH resulted in higher RCY, most notably at 10^{-6} M and 10^{-7} M ligand concentration—a molar activity of 28.2 GBq/μmol was achieved. Figure 4d illustrates a unique feature of H_6dappa—not only is there no difference between RCY at ambient temperature versus 50 °C labeling experiments, but under both conditions maximum radiolabeling occurs after just 1 min. Indeed, this characteristic could translate well into a clinical setting—the current gold-standard (DOTA) requires high

Table 2. Stepwise Stability Constants (log K) of H_6dappa with In^{3+}, Lu^{3+}, Sc^{3+}, and Y^{3+}

Equilibrium reaction	In^{3+}	Lu^{3+}	Sc^{3+}	Y^{3+}
M + L ⇆ ML	27.39(2)[a]; 27.55(5)[b]	18.35(3)[a], 18.71(5)[b]	22.86(4)[a]; 22.75(3)[d]	16.50(3)[a]; 16.79(6)[d]
ML + H^+ ⇆ MHL	4.81(2)[a]; 4.82(5)[b]	4.73(5)[a], 5.19(5)[b]	4.75(4)[a]; 4.69(3)[d]	4.83(4)[a]; 4.56(6)[d]
MHL + H^+ ⇆ MH_2L	4.43(4)[c]; 3.99(6)[b]	3.72(2)[c], 3.79(5)[b]	3.20(5)[a]; 3.69(5)[d]	3.96(3)[c]; 4.12(8)[d]
MH_2L + H^+ ⇆ MH_3L			1.26(6)[c]	
ML(OH) + H^+ ⇆ ML	9.67(3)[a]; 9.78(5)[b]	9.89(4)[a]	9.23(6)[a]; 9.42(5)[d]	9.55(4)[a]; 9.46(8)[d]
pM[e]	**27.7**	**18.6**	**23.2**	**16.8**

[a]Potentiometric and spectrophotometric titrations, I = 0.16 M (NaCl) and 298 K. [b]Ligand−ligand potentiometric competition with H_6ttha, I = 0.16 M (NaCl), 298 K. [c]In-batch acidic spectrophotometric titration, T = 298 K. [d]Ligand−ligand potentiometric competition with H_4edta at I = 0.16 M (NaCl), 298 K. [e]pM is defined as $-\log[M]_{free}$ at [L] = 10 μM, [M] = 1 μM, and pH 7.4. Charges omitted for clarity.

https://dx.doi.org/10.1021/acs.inorgchem.0c00671
Inorg. Chem. XXXX, XXX, XXX−XXX

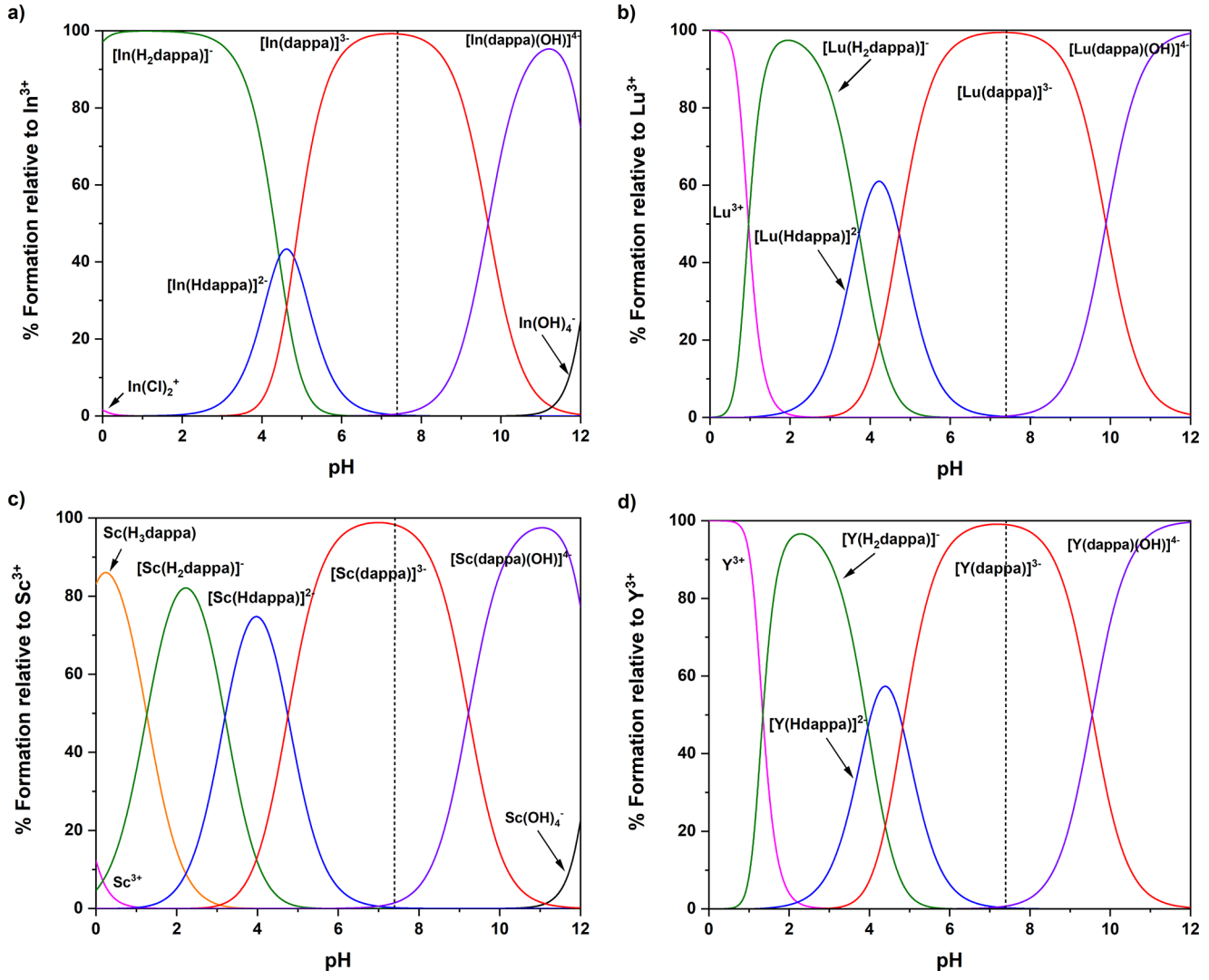

Figure 2. Speciation diagrams for H_6dappa complexes calculated from values in Table 2 (298 K, I = 0.16 M NaCl); dashed lines indicate physiological pH (7.4) (conditions simulated with HySS: [H_6dappa] = 1 mM, [M^{3+}] = 1 mM).

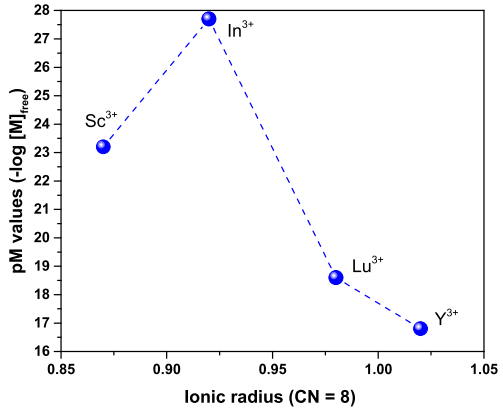

Figure 3. pM values versus ionic radii for $[M(dappa)]^{3-}$ complexes (CN = 8).

temperature (95 °C) and a long waiting period (~30 min) to radiolabel. These early studies suggest that H_6dappa radiolabeling with $[^{111}In]In^{3+}$ is slightly superior than with $[^{177}Lu]Lu^{3+}$. Similar time-, temperature-, pH-, and concentration-dependent labeling was observed, with the 95% RCY at pH 7 to obtain molar activity of 29.8 GBq/μmol being the most notable trial. It was hypothesized that studies with $[^{90}Y]Y^{3+}$ would be the least successful due to discouraging thermodynamic parameters with $[^{nat}Y]Y^{3+}$ in the solution studies. While, at high ligand concentration, RCYs in the realm of 90% were observed, a sharp decrease in RCY was noted even at [L] = 10^{-5} M. As the main difference between Y^{3+} and Lu^{3+} is the ionic radius, which is quite stark due to the well-known lanthanide contraction,[50] it is speculated that the size of yttrium is poorly suited to the binding cavity of H_6dappa.

The combination of encouraging results from thermodynamic studies and RCY optimization with $[^{nat/111}In]In^{3+}$ (respectively) led us to conduct human serum challenge experiments with $[^{111}In][In(dappa)]^{3-}$. The complex was formed at pH 7.5, diluted with PBS buffer, and then incubated in equal volume human serum proteins. PD-10 size-exclusion desalting columns were used to separate $[^{111}In][In(dappa)]^{3-}$ from serum-bound $[^{111}In]In^{3+}$. Aliquots were taken at 1, 48, 72, 96, and 120 h to yield a time-dependent plot describing the percentage of intact complex remaining in solution. Table 3 illustrates the rapid decomplexation of $[^{111}In][In(dappa)]^{3-}$, where after just 1 h nearly half of the initial $[^{111}In]In^{3+}$ becomes associated with competing serum proteins. Decom-

https://dx.doi.org/10.1021/acs.inorgchem.0c00671
Inorg. Chem. XXXX, XXX, XXX−XXX

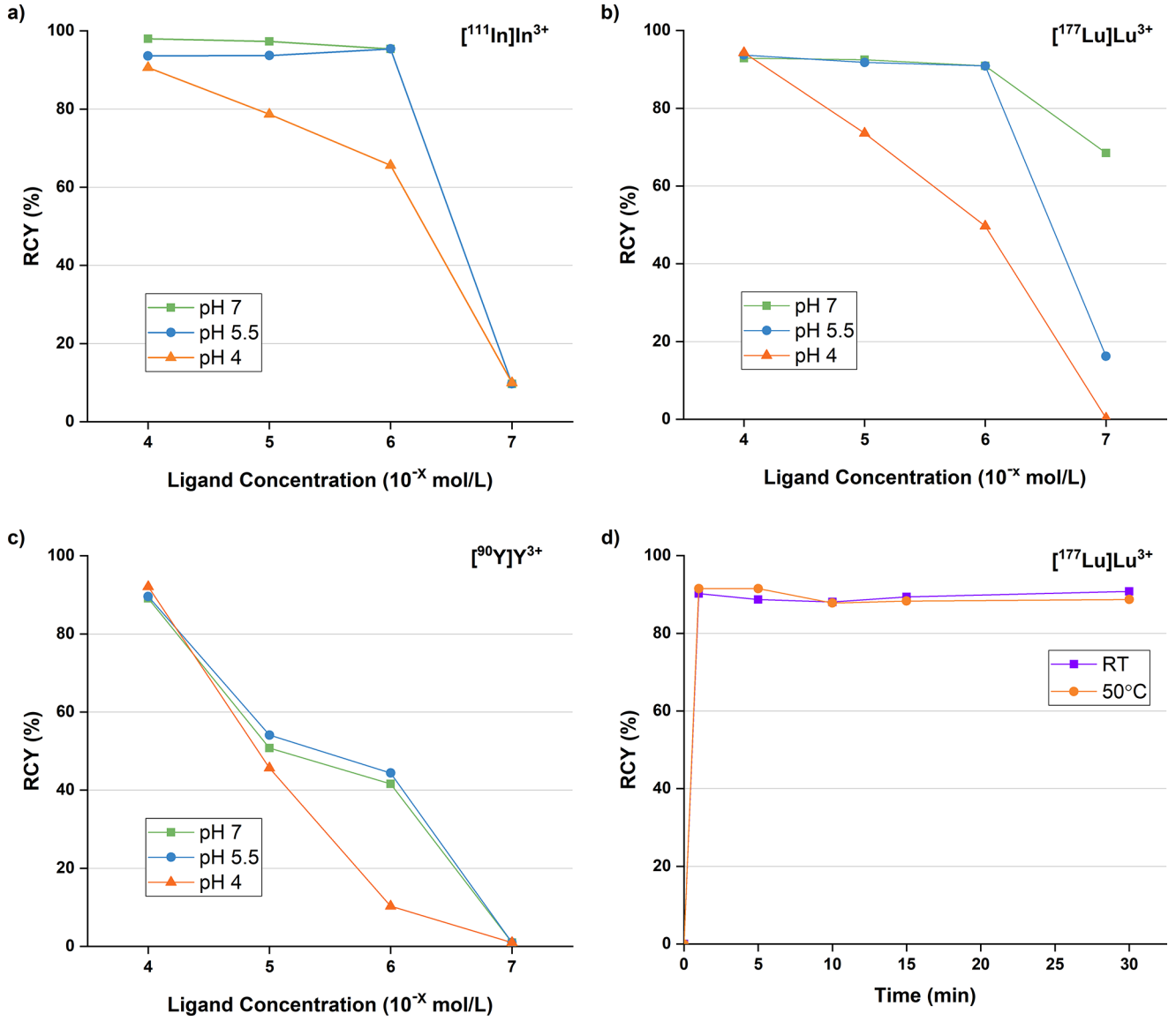

Figure 4. Concentration- and pH-dependent radiolabeling of H_6dappa (10 min, RT) in NH_4OAc solution (0.1 M) with (A) $[^{111}In]In^{3+}$, (B) $[^{177}Lu]Lu^{3+}$, and (C) $[^{90}Y]Y^{3+}$. (D) Time- and temperature-dependent radiolabeling of H_6dappa (10^{-5} M) in NH_4OAc solution (0.1 M, pH 5) with $[^{177}Lu]Lu^{3+}$.

Table 3. Serum Stability of $[^{111}In][In(dappa)]^{3-}$

Time (h)	Stability (%)[a]
1	53 ± 1
48	44 ± 2
72	41 ± 1
96	35 ± 1
120	31 ± 2

[a]Experiments done in triplicate. 37 MBq (1 mCi) quantitatively labeled with 10^{-5} M $Hdappa^{5-}$ (pH 7.5) then mixed with an equal volume of human serum and incubated at 37 °C. PD10 size exclusion columns used to separate intact complexes versus transchelated radiometal ions.

plexation continues at a slower rate for the next 5 days. Figure S36 illustrates a comparison of ^{111}In-dappa stability with "gold standard" ligands DOTA, CHX-A″-DTPA, and H_4octapa. The low kinetic inertness of the H_6dappa complex is easily rationalized when considering the rate of radiolabeling. The kinetic barrier toward complex formation must be low for such rapid labeling to occur; while this is beneficial during formation, it inherently leads to an easily transmetalated complex due to kinetic lability. If injected into a mammal, this would translate into (undesirable) off-target dose. Moreover, indirect evidence of instability can be found in RCY optimization data, as TLC peak tailing can be a sign of decomplexation. This observation may be a surprise considering the high thermodynamic stability of In-dappa (*vide supra*); however, in reality it appropriately highlights the fact that thermodynamic stability constants are not predictors of kinetic inertness or *in vivo* stability (as described elsewhere).[51,52] Indeed, the large difference in pIn between H_6dappa and DOTA (27.7 vs 18.8, respectively) is effectively irrelevant with respect to kinetic inertness. This is not to say that thermodynamic stability is not necessary for BFCs, but rather, above a certain (undefined) threshold, the magnitude of stability is less crucial.

Density Functional Theory Calculations. The structures and coordination geometry of aforementioned metal com-

https://dx.doi.org/10.1021/acs.inorgchem.0c00671
Inorg. Chem. XXXX, XXX, XXX−XXX

plexes (i.e., Sc^{3+}, In^{3+}, Y^{3+}, Lu^{3+}, and La^{3+}) in solution were studied using DFT calculations. The results are summarized in Figures 5 and S37. Aliphatic carboxylates in some structures (Figure S37) have been omitted for simplicity.

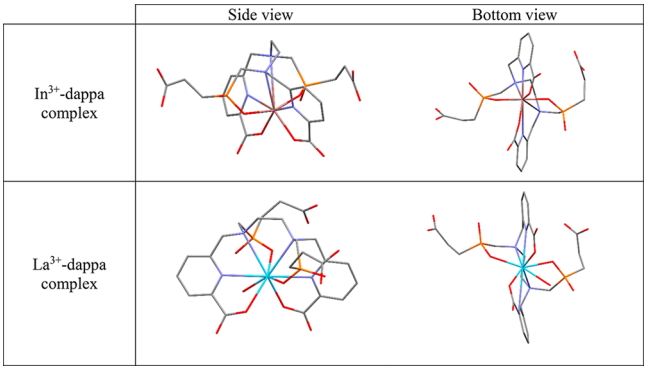

Figure 5. Structures of selected DFT calculated metal complexes.

The calculated In^{3+} complex reveals coordination of all 8 donor atoms (N_4O_4) with distorted square antiprism geometry, resulting in a symmetric structure. To gain additional insight into the kinetic inertness of $[^{111}In][In(dappa)]^{3-}$, we compared our calculated structure with the similar but more inert $[In(octapa)]^-$.[30] These results are summarized in Table 4 and Movie S1. As shown in the latter, the metal coordination geometries of the two structures are almost identical, with the main differences arising from the geometric and electronic influence of the phosphinate groups—the bite angle of phosphinate is known to be larger than that of carboxylate. Not only does this induce strain within the five membered N−In−OP coordination ring, but the steric constraint on the backbone also prevents the picolinic acids from conforming to the highly favorable twisted conformation (illustrated in Figure 2 of Boros et al.[49]). The asymmetry of coordinative bond lengths (Table 4) is also likely a result of this steric strain. In terms of electronics, the hardness of the phosphinate groups draws the In^{3+} away from the backbone and pyridine amines and closer to the picolinic acid groups (relative to $[In(octapa)]^-$) resulting in shallower encapsulation of the metal ion within the binding pocket. Calculated coordinative bond lengths support this assertion and can be found in Table 4.

Table 4. Comparison of DFT Calculated In−O and In−N Bond Lengths in In-octapa and In-dappa Complexes

In^{3+}-octapa			In^{3+}-dappa		
Atom 1	Atom 2	Length (Å)	Atom 1	Atom 2	Length (Å)
In	N1	2.9416	In	N1	2.6227
In	N2	2.9309	In	N2	3.7031
In	N3	2.3387	In	N3	3.0942
In	N4	2.3423	In	N4	2.2961
In	O1	2.1098	In	O1	2.1749
In	O2	2.1128	In	O2	2.0946
In	O3	2.1607	In	O3	2.0218
In	O4	2.1578	In	O4	2.0600

NMR spectra of In-dappa at physiological pH (Figure S11) point to the presence of fluxional isomers, as indicated by broad peaks in the ^1H NMR spectrum and a single broadened peak in the ^{31}P NMR spectrum. In addition to the structure shown in Figure 5 (minimum energy isomer), additional structures and their energies have been calculated (Figure S37) to explore the isomers responsible for this fluxionality. Coordination of both picolinic acid groups is supported by the single set of aromatic peaks in the ^1H NMR spectrum; thus, the ultimate goal of these calculations was to determine which two of the six remaining coordinating groups can reasonably be noncoordinating (since $CN_{In} = 8$).[34] All calculations with noncoordinating backbone amines either failed or were too energetically unfavorable, confirming a dedpa-like (*N*,*N*′-dipicolinate ethylene diamine) metal binding pocket.[49] Calculations with one or both carboxylic acids replacing adjacent phosphinates in the In^{3+} coordination sphere yielded reasonable geometries and energies, allowing us to conclude that NMR spectra broadness is likely a result of fluxional coordination between phosphinate and aliphatic carboxylic groups.

Taken together, we propose strained geometry, poor metal ion embedment within the binding cavity, and complex fluxionality at physiological pH all contribute to the rapid dissociation of $[^{111}In][In(dappa)]^{3-}$ observed during serum stability experiments

The La^{3+}-dappa complex (Figure 5) is also of interest due to its distinct differences from previously reported octadentate ligand complexes, $[La(octapa)]^-$ and $[La(octox)]^-$.[38,42] These octadentate ligands (N_4O_4) encapsulate La^{3+} while two water molecules coordinatively saturate the resulting decadentate metal ion. Conversely, due to crowding around the oxygen coordinating plane of La^{3+}, the dappa complex only permits coordination of one water molecule, resulting in a nonadentate metal ion. Furthermore, in agreement with ^1H and ^{31}P NMR spectra, the optimized DFT structure is symmetrical.

CONCLUSIONS

H_6dappa was successfully synthesized and fully characterized; its metal ion chelation was studied with a number of metal ions (In^{3+}, Lu^{3+}, Y^{3+}, Sc^{3+}, La^{3+}, Bi^{3+}), chosen based on the respective existence of radioisotopes that are of clinical interest for nuclear medicine. Metal chelation was first studied with NMR to confirm the formation of metal complexes, as well as gain insight into the degree of symmetry and/or disorder of the molecule. It was observed that the La^{3+} and In^{3+} complexes were highly symmetrical, evidenced by the clear diastereotopic splitting in the ^1H NMR spectra. Conversely, Bi^{3+}, Y^{3+}, Lu^{3+}, and Sc^{3+} complexes exhibited increasingly convoluted ^1H NMR spectra, likely as a result of the formation of multiple isomers. Solution studies (potentiometric and spectrophotometric titrations) were undertaken to probe the protonation constants of H_6dappa and thermodynamic stability of its complexes with In^{3+}, Lu^{3+}, Y^{3+}, and Sc^{3+}. Speciation diagrams, formation constants, and pM values were calculated. In each case, only one species predominated at physiological pH (7.4). The In^{3+} complex demonstrated the highest formation constant ($\log K_{ML} = 27.5$) and pM value (27.7), making it the most stable complex of the four studied. Radiolabeling experiments were conducted to investigate the highest molar activity achievable with three clinically relevant radionuclides ($[^{111}In]In^{3+}$, $[^{177}Lu]Lu^{3+}$, $[^{90}Y]Y^{3+}$). As expected, these results mimicked those found during solution studies. High molar activity was observed when radiolabeling $[^{111}In]In^{3+}$ with H_6dappa, with the maximum of 29.8 GBq/μmol occurring at $[H_6dappa] = 10^{-6}$ M with a RCY > 95%. Studies with

https://dx.doi.org/10.1021/acs.inorgchem.0c00671
Inorg. Chem. XXXX, XXX, XXX−XXX

[^{177}Lu]Lu^{3+} also yielded high molar activity (28.2 GBq/μmol at [H_6dappa] = 10^{-6} M with a RCY > 90%). The formation constant and pM value of Y^{3+}-dappa were the lowest of the studied metal ions, and similarly the radiolabeling of [^{90}Y]Y^{3+} resulted in the lowest RCYs and molar activities. Very mild and rapid radiolabeling was observed for all radionuclides studied, as only 1 min at room temperature was required to reach the maximum RCY. The kinetic inertness of the [$^{111}In^{3+}$][In(dappa)]$^{3-}$ complex was explored via serum stability studies. It was observed that rapid decomplexation occurred upon introduction of human serum proteins to a solution containing [^{111}In][In(dappa)]$^{3-}$, with near 50% degradation in 1 h, an outcome highlighting that thermodynamic stability is not a valid predictor or kinetic inertness or *in vivo* stability. DFT calculations revealed the rapid dissociation is likely a result of poor encapsulation of [^{111}In]In^{3+} in the binding pocket of H_6dappa. This is unlike what has previously been observed with H_4octapa,[30] leading to the conclusion that the replacement of carboxylic acids with phosphinates has an undesirable kinetic effect for "pa" family targeted radionuclide delivery, likely as a result of the steric and electronic effects of these newly introduced functional groups. Moreover, coordination by the aliphatic carboxylic acids likely results in the formation of fluxional isomers at physiological pH; future studies with amide-functionalized H_6dappa are of further interest to probe the influence of these proximal acid groups. Overall, H_6dappa may be better suited for applications requiring rapid metal coordination.

EXPERIMENTAL SECTION

Materials and Methods. All solvents and reagents were purchased from commercial suppliers (Sigma-Aldrich, Fisher Scientific, TCI America, Alfa Aesar, AK Scientific, Fluka) and were used as received. Human serum was purchased frozen from Sigma-Aldrich. Synthetic reactions were monitored by TLC (MERCK Silicagel 60 F254, aluminum sheet). Radiolabeling reactions were monitored by TLC (Silicagel 60 RP-18 F254S, aluminum sheet) and HPLC (Knauer Smartline System consisting of Smartline 1000 pump, K2501 diode array detector, Raytest Ramona Star activity detector, Chromgate 2.8 software and a Smartline 5000 manager with a Zobax SB-C18 column; Agilent 4.6 × 250 mm, 5 μm). Radio-TLC chromatograms were scanned using a radioisotope thin layer analyzer (BIOSCAN system 200 imaging scanner, Rita Star or Fuji BAS-1800II, raytest); evaluation program AIDA. Flash chromatography was performed using Redisep Rf HP silica columns and a Teledyne Isco (Lincoln, NE) Combiflash Rf automated system. Water used was ultrapure (18.2 MΩ cm^{-1} at 298 K, Milli-Q, Millipore, Billerica, MA). ^{1}H, ^{13}C{^{1}H}, and ^{31}P{^{1}H} NMR spectra were recorded at ambient temperature on Bruker AV300 and AV400 instruments; unless otherwise specified the NMR spectra are expressed on the δ scale and referenced to residual solvent peaks. Low resolution (LR) mass spectrometry was performed using a Waters ZG spectrometer with an ESCI electrospray/chemical-ionization source, and high-resolution electrospray ionization mass spectrometry (HR-ESI-MS) was performed on a Micromass LCT time-of-flight instrument at the Department of Chemistry, University of British Columbia. Microanalyses for C, H, and N were performed on a Carlo Erba elemental analyzer EA 1108. The HPLC system used for analysis and purification of nonradioactive compounds consisted of a Waters 600 controller, A Waters 2487 dual wavelength absorbance detector and a Waters delta 600 pump with a Phenomenex Synergi 4 μm hydro-RP 80 Å column (250 mm × 21.2 mm semipreparative) or a Zorbax (Agilent) 300SB-C18, 300 Å, 5 μm, 9.4 mm × 250 mm column were used for purification of H_6dappa (**6**). $^{111}InCl_3$ was cyclotron-produced [^{112}Cd(p,2n)^{111}In; no carrier added; Fe, Cd, Cu, Pb, Zn, Ni each ≤100 ng/mCi] and purchased from BWX Technologies as 0.05 M HCl solution or from Curium Pharma as 0.02 M HCl solution. $^{177}LuCl_3$ was produced by reactor-based indirect strategy[53,54] [^{176}Yb(n,γ)^{177}Yb → ^{177}Lu, no carrier added; specific activity 3800−3000 GBq/mg] and was purchased from ITG (Isotope Technologies Garching) GmbH as 0.04 M HCl solution. $^{90}YCl_3$ [^{90}Sr/^{90}Y generator; carrier free] was purchased from Eckert & Ziegler Strahlen- and Medizintechnik AG as 0.04 M HCl solution. Radionuclide solutions were used within one-half-life (upon arrival) to minimize reduction in specific activity.

Synthesis and Characterization. *Methyl-6-bromomethylpicolinate (**1**).* Compound **1** was prepared according to the literature preparation with appropriate characteristic spectra.[55]

*(2-Carboxyethyl)phosphinic Acid (**2**).* Compound **2** was prepared according to the literature preparation with appropriate characteristic spectra.[33]

*N,N′-Dibenzylethane-1,2-diamine·2HCl (**3**).* Ethylene diamine (3.00 g, 3.34 mL, 49.9 mmol) and benzaldehyde (11.7 g, 11.2 mL, 110 mmol) were dissolved in MeOH (150 mL) in a round-bottom flask. The solution was stirred and heated to reflux for 5 h, during which time the yellow solution darkened into a yellow-orange color. The solution was then allowed to cool to ambient temperature and then cooled to 0 °C in an ice bath. $NaBH_4$ (6.61 g, 175 mmol) was added in several portions, and the solution was allowed to warm to ambient temperature and stirred for 24 h. After LR-MS revealed complete reduction of the imine intermediate, the solution was evaporated via rotary evaporator to yield a yellow oil. Aqueous HCl (3 M, 50 mL) was slowly added to the oil to yield a white solid that was filtered out and washed with acetone to yield **3** as a dihydrochloric acid salt (13.1 g, 95%). ^{1}H NMR (300 MHz, 298 K, D_2O + NaOD): δ 7.51−7.46 (m, 10H), 4.23 (s, 4 H), 3.37 (s, 4H). ^{13}C{^{1}H} NMR (100 MHz, 298 K, D_2O + NaOD): 131.3, 129.6, 129.6, 129.3, 51.6, 43.0. LR-ESI-MS: calcd for [$C_{16}H_{20}N_2$ + H]$^+$: 241.2; found [M + H]$^+$: 241.3. Elemental analysis: calcd % for $C_{16}H_{20}N_2$·2HCl: C 61.35, H 7.08, N 8.94; found: C 61.67, H 6.93, N 8.94.

*Dimethyl-6,6′([ethane-1,2-diylbis{benzylazanediyl}]bis-[methylene])dipicolinate (**4**).* Compounds **1** (3.40 g, 14.7 mmol) and **3** (1.87 g, 5.97 mmol) were dissolved in ACN (120 mL) in a round-bottom flask. K_2CO_3 (5.61 g, 40.6 mmol) was then added, and the solution was stirred and heated to reflux for 3 d. The reaction mixture was quenched with H_2O (100 mL), and then DCM (140 mL) was added for the first extraction. The phases were separated and the aqueous phase was further washed with DCM (3 × 100 mL); the combined organic phases were dried over $MgSO_4$, filtered, and loaded onto Celite and dried. The product was purified via column chromatography using a silica column (CombiFlash R_f automated column system, 120 g gold silica column, 100% hexane to 100% EtOAc). The product fractions were rotary evaporated to yield an oil, which solidified to a yellow solid upon standing at ambient temperature (1.82 g, 57%). ^{1}H NMR (400 MHz, 298 K, $CDCl_3$): δ 7.95 (t, J = 4.4 Hz, 1H), 7.69 (d, J = 4.5 Hz, 2H), 7.30−7.15 (m, ∼5H; overlap with $CDCl_3$), 3.97 (s, 3H), 3.82 (s, 2H), 3.57 (s, 2H), 2.68 (s, 2H). ^{13}C{^{1}H} NMR (100 MHz, 298 K, $CDCl_3$): 165.8, 161.1, 147.1, 139.0, 137.3, 128.7, 128.3, 127.0, 125.9, 123.5, 60.5, 59.1, 52.9, 52.0. LR-ESI-MS: calcd for [$C_{32}H_{34}N_4O_4$ + H]$^+$: 539.3; found [M + H]$^+$: 539.3.

*Dimethyl-6,6′-([ethane-1,2-diylbis{azanediyl}]bis[methylene])-dipicolinate (**5**).* Compound **4** (1.18 g, 2.19 mmol) was dissolved in 50 mL of glacial acetic acid in a two-neck round-bottom flask. The flask was purged with N_2 and 10% w/w Pd/C (375 mg, 0.35 mmol) added under a stream of N_2. The flask was thrice purged with N_2 and then filled with H_2 from a balloon. The mixture was stirred at room temperature overnight under H_2, and then Pd/C was removed by filter paper, which was washed alternately with ACN (3 × 30 mL) and 3 M aqueous HCl (2 × 10 mL). The solution was evaporated and the dark orange oil dissolved in minimal ACN and then run through a small Celite plug to remove residual Pd/C. The solvent was removed by rotary evaporator with EtOH added and evaporated twice to remove residual acetic acid. Following *in vacuo* solvent removal, the dark orange oil solidified (712 mg, 90%) and was used without further purification. ^{1}H NMR (400 MHz, 298 K, D_2O): δ 8.20 (d, J = 7.4 Hz,

https://dx.doi.org/10.1021/acs.inorgchem.0c00671
Inorg. Chem. XXXX, XXX, XXX−XXX

1H), 8.12 (t, J = 7.8 Hz, 1H), 7.75 (d, J = 7.7 Hz, 1H), 4.70 (s, 2H), 3.91 (s, 3H), 3.73 (s, 2H). $^{13}C\{^1H\}$ NMR (100 MHz, 298 K, D_2O): 166.7, 151.1, 146.5, 140.0, 127.4, 125.7, 53.5, 50.6, 43.9. LR-ESI-MS: calcd for $[C_{18}H_{22}N_4O_4 + H]^+$: 359.2; found $[M + H]^+$: 359.1.

H_6dappa (6). Compounds **5** (500 mg, 1.40 mmol) and **2** (773 mg, 5.60 mmol) were added to 6 M HCl (1.5 mL) in a two-dram (7.4 mL) vial. Upon heating to 80 °C the components dissolved to yield a brownish-orange solution. Over the course of 24 h, paraformaldehyde (628 mg, 20.9 mmol) was added in small portions. After full addition of the paraformaldehyde, the solution was refluxed for an additional 24 h. The solvent was removed by rotary evaporator and most of the remaining HCl removed by repeatedly adding small portions of water and then evaporating to dryness. The dark brown oil was dissolved in water (5 mL) and neutralized with 1 M NaOH. The crude product was first purified by chromatography on ion-exchange resin (DOWEX 50W2, H^+-form, 100−200 mesh; column size 32 cm × 2 cm; eluent: water). Impurities were removed with the first 200 mL of eluate. The next 250 mL of eluate, containing semipure product, was collected and the solvent removed by rotary evaporator. The pale yellow oil was dissolved in water (2 mL) and purified by HPLC (Phenomenex Synergi 4 μm hydro-RP 80 Å column, 250 mm × 21.2 mm semipreparative; A: H_2O 0.1% TFA, B: ACN, 100% A to 85% A−15% B over 20 min, maintain 85% A−15% B for 5 min. t_R = 22.6 min). Pure fractions were combined, evaporated to ∼3−5 mL, and lyophilized to yield pure product as a fluffy white powder (241 mg, 18%). ^1H NMR (400 MHz, 298 K, D_2O): 8.04 (t, J = 7.8 Hz, 1H), 7.97 (d, J = 7.7 Hz, 1H), 7.69 (d, J = 7.7 Hz, 1H), 4.42 (s, 2H), 3.51 (s, 2H), 3.15 (d, J = 7.4 Hz, 2H), 2.20 (dt, J_3^{PH} = 12.6 Hz, J_3^{HH} = 7.8 Hz, 2H), 1.68 (dt, J_2^{PH} = 14.9 Hz, J_3^{HH} = 7.8 Hz, 2H). $^{13}C\{^1H\}$ NMR (100 MHz, 298 K, D_2O): 176.2 (d, J = 14.3 Hz), 164.9, 151.3, 144.8, 143.2, 129.1, 126.1, 58.0, 52.4, 52.3 (d, J = 92.8 Hz), 26.3 (d, J = 3.2 Hz), 24.2 (d, J = 96.5 Hz). $^{31}P\{^1H\}$ NMR (162 MHz, 298 K, D_2O, externally referenced to 85% phosphoric acid): 33.91. HR-ESI-MS: calcd for $[C_{24}H_{32}N_4O_{12}P_2 + H]^+$: 631.1570; found $[M + H]^+$: 631.1572. Elemental analysis: calcd % for H_6dappa·2.6TFA·1.8H_2O: C 36.56, H 4.01, N 5.84; found: C 36.61, H 4.08, N 5.79.

Metal Complexation. NMR spectra of $[M(H_x\text{dappa})]^{3-x}$ (M = In^{3+}, Lu^{3+}, Y^{3+}, Sc^{3+}, La^{3+}; x = 2, 1, 0, −1) were obtained by making separate ligand and metal solutions in D_2O (5−20 mM) and then mixing the solutions in a molar ratio of 1:1.1/L:M (V_t > 300 μL). If necessary, solution pD was altered with freshly prepared ∼0.1 M NaOD (diluted from 40 wt % NaOD) and measured with a Ross combined electrode and corrected pD = $pH_{measured}$ + 0.4. Solutions were allowed to stand for at least 5 min at room temperature before collecting NMR spectra. Due to the poor solubility of $Bi(NO_3)_3\cdot 5H_2O$ in neutral D_2O, for $[Bi(H_x\text{dappa})]^{x-3}$, the desired amount of $Bi(NO_3)_3\cdot 5H_2O$ was weighed on an analytical balance and then a 1:1.1 (L:M) molar ratio of $dappa^{6-}$ solution was added to the metal salt. Following dissolution of the solid, D_2O was used to dilute the solution by a factor of 2.

Solution Thermodynamics. All potentiometric titrations were carried out with a Metrohm Titrando 809 and a Metrohm Dosino 800 with a Ross combined electrode. A 20 mL 298 K thermostated glass cell with an inlet—outlet tube for nitrogen gas (purified through a 10% NaOH solution to exclude CO_2 prior to and during the course of the titration) was used as a titration cell. The electrode was calibrated daily in hydrogen ion concentration by direct titration of HCl with freshly prepared NaOH solution, and the results were analyzed with the Gran procedure[56] in order to obtain the standard potential (E^o) and the ionic product of water pK_w, T = 298 K, and 0.16 M NaCl as a supporting electrolyte. Solutions were titrated with carbonate-free NaOH (∼0.16 M) that was standardized against freshly recrystallized potassium hydrogen phthalate. The experimental procedures for determination of the ligand protonation constants, complex formation, and pM values are described in the Supporting Information.

Radiolabeling and Human Serum Challenge Experiments. For concentration-dependent radiolabeling, an aliquot of a ligand solution (25 μL) of desired concentration was mixed with $[^{90}Y]Y^{3+}$or $[^{111}In]In^{3+}$ or $[^{177}Lu]Lu^{3+}$ (7.5 MBq, 0.2 mCi) and diluted to a final volume (250 μL) with ammonium acetate solution (0.1 M, pH = 2, 4, 5.5, 7, or 7.5). The final mixture was incubated at room temperature or 50 °C for the specific amount of time (i.e., 1, 5, 10, 15, or 30 min) before determination of radiochemical yield. Initial attempts to quantify RCY with HPLC (Zorbax SB-C18 column; Agilent 4.6 × 250 mm, 5 μm; solvent A = H_2O 0.1% TFA, solvent B = ACN 0.1% TFA) were unsuccessful due to the expected high hydrophilicity of the many $dappa^{6-}$ metal complexes, resulting in identical retention times for the free ligand and metal complexes (which eluted at the solvent front; Figure S32). Accordingly, RP-18 silicagel TLC plates were used to quantify RCY—typically 2−5 μL was spotted per plate. NH_4OH/MeOH/H_2O (1/10/20) was used as a mobile phase for TLC. As seen in Figures S33−S35, in the absence of $dappa^{6-}$ (denoted "control") the free radiometal remained at the baseline of the TLC plate. When $dappa^{6-}$ was present, the activity moved up the TLC plate, with the degree of streaking being dependent on the radiometal ion under investigation. For the human serum challenge, GE Healthcare Life Sciences PD-10 desalting columns (size exclusion for MW < 5000 Da) and a Capintec CRC 55t dose calibrator were used, as was previously described.[48] Briefly, 37 MBq (1 mCi) of $[^{111}In]In^{3+}$ was near-quantitatively labeled with 10^{-5} M H_6dappa (pH 7.5), diluted to 1 mL with PBS buffer, and then mixed with an equal volume of human serum and incubated at 37 °C. Aliquots were taken at 1 h, 2 d, 3 d, 4 d, and 5 d. Aliquots were diluted to 2.5 mL with PBS, loaded onto a conditioned PD-10 column, and eluted with an additional 3.5 mL of PBS. The activity of the vial containing the diluted aliquot was measured prior to loading of the column (initial activity), as well as following loading (residual activity). Stability was calcuated through eq 1.

$$\text{stability} = 1 - (\text{eluted activity}/(\text{initial activity} - \text{residual activity})) \quad (1)$$

Density Functional Theory Calculations. All DFT calculations were performed as implemented in the Gaussian 09 revision D.01 suite of ab initio quantum chemistry programs (Gaussian Inc., Wallingford, CT)[57] and visualized using Mercury 4.1. The structure geometry was optimized using the TPSSh functional,[58] TZVP basis set[59] for first- and second-row elements. The Stuttgart/Dresden and associated effective core potentials's basis set was used for In and La,[60,61] in the presence of water solvent (IEF PCM as implemented in G09) without the use of symmetry constraints.

■ ASSOCIATED CONTENT

Supporting Information

The Supporting Information is available free of charge at https://pubs.acs.org/doi/10.1021/acs.inorgchem.0c00671.

Representative spectra of the in-batch UV-titrations of M^{3+}-dappa (M = In, Lu, Sc, Y) systems as the pH is raised; stepwise protonation constants (log K) of M^{3+}-dappa (M = In, Lu, Sc, Y) complexes; NMR spectra (^1H, $^1H\{^{31}P\}$, $^{31}P\{^1H\}$, $^{13}C\{^1H\}$, COSY) and high resolution mass spectra of metal complexes; radiochemical yield data ($^{111}In^{3+}$, $^{177}Lu^{3+}$, $^{90}Y^{3+}$) and radio-HPLC ($^{111}Lu^{3+}$) spectra of radiometal complexes. (PDF)

Comparison of the structures of $[^{111}In][In(dappa)]$ and $[In(octapa)]^-$ (MPG)

■ AUTHOR INFORMATION

Corresponding Authors

María de Guadalupe Jaraquemada-Peláez − *Medicinal Inorganic Chemistry Group, Department of Chemistry, University of British Columbia, Vancouver, British Columbia V6T 1Z1, Canada;* orcid.org/0000-0002-6204-707X; Email: mdgjara@chem.ubc.ca

Chris Orvig − *Medicinal Inorganic Chemistry Group, Department of Chemistry, University of British Columbia,*

https://dx.doi.org/10.1021/acs.inorgchem.0c00671
Inorg. Chem. XXXX, XXX, XXX−XXX

Vancouver, British Columbia V6T 1Z1, Canada; orcid.org/0000-0002-2830-5493; Email: orvig@chem.ubc.ca

Authors

Thomas I. Kostelnik − *Medicinal Inorganic Chemistry Group, Department of Chemistry, University of British Columbia, Vancouver, British Columbia V6T 1Z1, Canada; Sciences Division, TRIUMF, Vancouver, British Columbia V6T 2A3, Canada*

Xiaozhu Wang − *Medicinal Inorganic Chemistry Group, Department of Chemistry, University of British Columbia, Vancouver, British Columbia V6T 1Z1, Canada;* orcid.org/0000-0002-5882-0066

Lily Southcott − *Medicinal Inorganic Chemistry Group, Department of Chemistry, University of British Columbia, Vancouver, British Columbia V6T 1Z1, Canada; Sciences Division, TRIUMF, Vancouver, British Columbia V6T 2A3, Canada*

Hannah K. Wagner − *Medicinal Inorganic Chemistry Group, Department of Chemistry, University of British Columbia, Vancouver, British Columbia V6T 1Z1, Canada; Anorganish-Chemisches Institut, Universität Heidelberg, 69120 Heidelberg, Germany*

Manja Kubeil − *Institute of Radiopharmaceutical Cancer Research, Helmholtz - Zentrum Dresden - Rossendorf, 01328 Dresden, Germany;* orcid.org/0000-0001-8857-5922

Holger Stephan − *Institute of Radiopharmaceutical Cancer Research, Helmholtz - Zentrum Dresden - Rossendorf, 01328 Dresden, Germany;* orcid.org/0000-0002-2972-2803

Complete contact information is available at: https://pubs.acs.org/10.1021/acs.inorgchem.0c00671

Author Contributions

The manuscript was written through contributions of all authors. All authors have given approval of the final version of the manuscript.

Notes

The authors declare no competing financial interest.

■ ACKNOWLEDGMENTS

We gratefully acknowledge the Natural Sciences and Engineering Research Council (NSERC) of Canada for CGS-M/CGS-D scholarships (TIK, LS) and NSERC CREATE IsoSiM at TRIUMF for Ph.D. research stipends (TIK, LS), both NSERC and CIHR for financial support via a Collaborative Health Research Project (CHRP - CO) as well as NSERC Discovery (CO). We also thank the University of British Columbia (UBC) for 4YF and Laird fellowships (TIK, LS). We gratefully acknowledge Maria Ezhova for her expert advice on NMR experiments at UBC and Karin Landrock for excellent technical assistance at HZDR. Helmholtz-Zentrum Dresden-Rossendorf is thanked for supporting the IsoSiM International Research Experience program; TRIUMF receives federal funding via a contribution agreement with the National Research Council of Canada. We thank WestGrid and Compute Canada for their resource support.

■ REFERENCES

(1) Kostelnik, T. I.; Orvig, C. Radioactive Main Group and Rare Earth Metals for Imaging and Therapy. *Chem. Rev.* **2019**, *119*, 902−956.

(2) Opacic, T.; Paefgen, V.; Lammers, T.; Kiessling, F. Status and Trends in the Development of Clinical Diagnostic Agents. *Wiley Interdiscip. Rev. Nanomed. Nanobiotech.* **2017**, *9*, e1441.

(3) Strosberg, J.; El-Haddad, G.; Wolin, E.; Hendifar, A.; Yao, J.; Chasen, B.; Mittra, E.; Kunz, P. L.; Kulke, M. H.; Jacene, H.; et al. Phase 3 Trial of ^{177}Lu-Dotatate for Midgut Neuroendocrine Tumors. *N. Engl. J. Med.* **2017**, *376*, 125−135.

(4) FDA approves lutetium Lu 177 dotatate for treatment of GEP-NETS. https://www.fda.gov/Drugs/InformationOnDrugs/ApprovedDrugs/ucm594105.htm (accessed 2020-02-01).

(5) Livechart - Table of Nuclides -Nuclear Structure and Decay Data. https://www-nds.iaea.org/relnsd/vcharthtml/VChartHTML.html (accessed 2020-02-01).

(6) Burke, B. P.; Seemann, J.; Archibald, S. J. Advanced Chelator Design for Metal Complexes in Imaging Applications. *Adv. Inorg. Chem.* **2016**, *68*, 301−339.

(7) Ramogida, C. F.; Orvig, C. Tumour Targeting with Radiometals for Diagnosis and Therapy. *Chem. Commun.* **2013**, *49*, 4720−4739.

(8) Price, E. W.; Orvig, C. Matching Chelators to Radiometals for Radiopharmaceuticals. *Chem. Soc. Rev.* **2014**, *43*, 260−290.

(9) Martell, A. E.; Hancock, R. D. *Metal Complexes in Aqueous Solutions*; Fackler, J. P., Ed.; Plenum Press: New York, 1996.

(10) Mitterhauser, M.; Toegel, S.; Wadsak, W.; Lanzenberger, R. R.; Mien, L.-K.; Kuntner, C.; Wanek, T.; Eidherr, H.; Ettlinger, D. E.; Viernstein, H.; et al. Pre Vivo, Ex Vivo and in Vivo Evaluations of [^{68}Ga]-EDTMP. *Nucl. Med. Biol.* **2007**, *34*, 391−397.

(11) Kolesnikov-Gauthier, H.; Lemoine, N.; Tresch-Bruneel, E.; Olivier, A.; Oudoux, A.; Penel, N. Efficacy and Safety of ^{153}Sm-EDTMP as Treatment of Painful Bone Metastasis: A Large Single-Center Study. *Support. Care Cancer* **2018**, *26*, 751−758.

(12) Agarwal, K. K.; Singla, S.; Arora, G.; Bal, C. ^{177}Lu-EDTMP for Palliation of Pain from Bone Metastases in Patients with Prostate and Breast Cancer: A Phase II Study. *Eur. J. Nucl. Med. Mol. Imaging* **2015**, *42*, 79−88.

(13) Sharma, S.; Singh, B.; Koul, A.; Mittal, B. R. Comparative Therapeutic Efficacy of ^{153}Sm-EDTMP and ^{177}Lu-EDTMP for Bone Pain Palliation in Patients with Skeletal Metastases: Patients' Pain Score Analysis and Personalized Dosimetry. *Front. Med.* **2017**, *4*, 46.

(14) Beaino, W.; Anderson, C. J. PET Imaging of Very Late Antigen-4 in Melanoma: Comparison of ^{68}Ga- and ^{64}Cu-Labeled NODAGA and CB-TE1A1P-LLP2A Conjugates. *J. Nucl. Med.* **2014**, *55*, 1856−1863.

(15) Price, E. W.; Zeglis, B. M.; Lewis, J. S.; Adam, M. J.; Orvig, C. H_6Phospa-Trastuzumab: Bifunctional Methylenephosphonate-Based Chelator with ^{89}Zr, ^{111}In and ^{177}Lu. *Dalton Trans.* **2014**, *43*, 119−131.

(16) Šimeček, J.; Hermann, P.; Seidl, C.; Bruchertseifer, F.; Morgenstern, A.; Wester, H.-J.; Notni, J. Efficient Formation of Inert Bi-213 Chelates by Tetraphosphorus Acid Analogues of DOTA: Towards Improved Alpha-Therapeutics. *EJNMMI Res.* **2018**, *8*, 78.

(17) Weekes, D. M.; Orvig, C. Harnessing the Bone-Seeking Ability of Ca(II)-like Metal Ions in the Treatment of Metastatic Cancer and Resorption Disorders. *Chem. Soc. Rev.* **2016**, *45*, 2024−2031.

(18) Kolesnikov-Gauthier, H.; Lemoine, N.; Oudoux, A.; Olivier, A.; Tresch-Bruneel, E.; Penel, N. Efficacy of Quadramet® (QUA) as Treatment of Painful Bone Metastasis: A Large Single-Center Study. *Ann. Oncol.* **2016**, *27*, vi456.

(19) Soodgupta, D.; Hurchla, M. A.; Jiang, M.; Zheleznyak, A.; Weilbaecher, K. N.; Anderson, C. J.; Tomasson, M. H.; Shokeen, M. Very Late Antigen-4 (A4β1 Integrin) Targeted PET Imaging of Multiple Myeloma. *PLoS One* **2013**, *8*, e55841.

(20) Abada, S.; Lecointre, A.; Christine, C.; Ehret-Sabatier, L.; Saupe, F.; Orend, G.; Brasse, D.; Ouadi, A.; Hussenet, T.; Laquerrière, P.; et al. Phosphonated Chelates for Nuclear Imaging. *Org. Biomol. Chem.* **2014**, *12*, 9601−9620.

(21) David, T.; Křečková, P.; Kotek, J.; Kubíček, V.; Lukeš, I. 1-Hydroxy-1,1-Bis(H-Phosphinates): Synthesis, Stability, and Sorption Properties. *Heteroat. Chem.* **2012**, *23*, 195−201.

(22) Prata, M. I. M.; Santos, A. C.; Geraldes, C. F. G. C.; Lima, J. J. P. d. Characterisation of $^{67}Ga^{3+}$ Complexes of Triaza Macrocyclic

https://dx.doi.org/10.1021/acs.inorgchem.0c00671
Inorg. Chem. XXXX, XXX, XXX−XXX

Ligands: Biodistribution and Clearance Studies. *Nucl. Med. Biol.* **1999**, *26*, 707−710.
(23) Prata, M. I. M.; André, J. P.; Kovács, Z.; Takács, A. I.; Tircsó, G.; Tóth, I.; Geraldes, C. F. G. C. Gallium(III) Chelates of Mixed Phosphonate-Carboxylate Triazamacrocyclic Ligands Relevant to Nuclear Medicine: Structural, Stability and in Vivo Studies. *J. Inorg. Biochem.* **2017**, *177*, 8−16.
(24) Notni, J.; Šimeček, J.; Hermann, P.; Wester, H. J. TRAP, a Powerful and Versatile Framework for Gallium-68 Radiopharmaceuticals. *Chem. - Eur. J.* **2011**, *17*, 14718−14722.
(25) Notni, J.; Pohle, K.; Wester, H.-J. Comparative Gallium-68 Labeling of TRAP-, NOTA-, and DOTA-Peptides: Practical Consequences for the Future of Gallium-68-PET. *EJNMMI Res.* **2012**, *2*, 1−5.
(26) Notni, J.; Pohle, K.; Wester, H. J. Be Spoilt for Choice with Radiolabelled RGD Peptides: Preclinical Evaluation of ^{68}Ga-TRAP-(RGD)$_3$. *Nucl. Med. Biol.* **2013**, *40*, 33−41.
(27) Kazmierczak, P. M.; Todica, A.; Gildehaus, F.-J.; Hirner-Eppeneder, H.; Brendel, M.; Eschbach, R. S.; Hellmann, M.; Nikolaou, K.; Reiser, M. F.; Wester, H.-J.; et al. ^{68}Ga-TRAP-(RGD)$_3$ Hybrid Imaging for the In Vivo Monitoring of $\alpha_v\beta_3$-Integrin Expression as Biomarker of Anti-Angiogenic Therapy Effects in Experimental Breast Cancer. *PLoS One* **2016**, *11*, e0168248.
(28) Šimeček, J.; Zemek, O.; Hermann, P.; Notni, J.; Wester, H.-J. Tailored Gallium(III) Chelator NOPO: Synthesis, Characterization, Bioconjugation, and Application in Preclinical Ga-68-PET Imaging. *Mol. Pharmaceutics* **2014**, *11*, 3893−3903.
(29) Šimeček, J.; Notni, J.; Kapp, T. G.; Kessler, H.; Wester, H.-J. Benefits of NOPO As Chelator in Gallium-68 Peptides, Exemplified by Preclinical Characterization of ^{68}Ga-NOPO−c(RGDfK). *Mol. Pharmaceutics* **2014**, *11*, 1687−1695.
(30) Price, E. W.; Cawthray, J. F.; Bailey, G. A.; Ferreira, C. L.; Boros, E.; Adam, M. J.; Orvig, C. H_4Octapa: An Acyclic Chelator for ^{111}In Radiopharmaceuticals. *J. Am. Chem. Soc.* **2012**, *134*, 8670−8683.
(31) Zhang, S.; Ibrahim, J. J.; Yang, Y. A Pincer Ligand Enabled Ruthenium Catalyzed Highly Selective N -Monomethylation of Nitroarenes with Methanol as the C1 Source. *Org. Chem. Front.* **2019**, *6*, 2726−2731.
(32) Goswami, S.; Sen, D.; Das, N. K. Metal Ion Based Chiral Fluorescence Sensor Selective for Dihydrogenphosphate. *Tetrahedron Lett.* **2010**, *51*, 6707−6710.
(33) Notni, J.; Hermann, P.; Havlíčková, J.; Kotek, J.; Kubíček, V.; Plutnar, J.; Loktionova, N.; Riss, P. J.; Rösch, F.; Lukeš, I. A Triazacyclononane-Based Bifunctional Phosphinate Ligand for the Preparation of Multimeric ^{68}Ga Tracers for Positron Emission Tomography. *Chem. - Eur. J.* **2010**, *16*, 7174−7185.
(34) Shannon, R. D. Revised Effective Ionic Radii and Systematic Studies of Interatomic Distances in Halides and Chalcogenides. *Acta Crystallogr., Sect. A: Cryst. Phys., Diffr., Theor. Gen. Crystallogr.* **1976**, *32*, 751−767.
(35) Gans, P.; Sabatini, A.; Vacca, A. Determination of Equilibrium Constants from Spectrophometric Data Obtained from Solutions of Known PH : The Program PHab. *Ann. Chim.* **1999**, *89*, 45−49.
(36) Gans, P.; Sabatini, A.; Vacca, A. Investigation of Equilibria in Solution. Determination of Equilibrium Constants with the HYPERQUAD Suite of Programs. *Talanta* **1996**, *43*, 1739−1753.
(37) Li, L.; Jaraquemada-Peláez, M.; de, G.; Kuo, H.-T.; Merkens, H.; Choudhary, N.; Gitschtaler, K.; Jermilova, U.; Colpo, N.; Uribe-Munoz, C.; Radchenko, V.; et al. Functionally Versatile and Highly Stable Chelator for ^{111}In and ^{177}Lu: Proof-of-Principle Prostate-Specific Membrane Antigen Targeting. *Bioconjugate Chem.* **2019**, *30*, 1539−1553.
(38) Jaraquemada-Peláez, M.; de, G.; Wang, X.; Clough, T. J.; Cao, Y.; Choudhary, N.; Emler, K.; Patrick, B. O.; Orvig, C. H_4Octapa: Synthesis, Solution Equilibria and Complexes with Useful Radiopharmaceutical Metal Ions. *Dalton Trans.* **2017**, *46*, 14647−14658.
(39) Alderighi, L.; Gans, P.; Ienco, A.; Peters, D.; Sabatini, A.; Vacca, A. Hyperquad Simulation and Speciation (HySS): A Utility Program for the Investigation of Equilibria Involving Soluble and Partially Soluble Species. *Coord. Chem. Rev.* **1999**, *184*, 311−318.
(40) Harris, W. R.; Carrano, C. J.; Raymond, K. N. Spectrophotometric Determination of the Proton-Dependent Stability Constant of Ferric Enterobactin. *J. Am. Chem. Soc.* **1979**, *101*, 2213−2214.
(41) Spreckelmeyer, S.; Ramogida, C. F.; Rousseau, J.; Arane, K.; Bratanovic, I.; Colpo, N.; Jermilova, U.; Dias, G. M.; Dude, I.; Jaraquemada-Peláez, M.; de, G.; et al. P-NO_2−Bn−H_4Neunpa and H_4Neunpa−Trastuzumab: Bifunctional Chelator for Radiometalpharmaceuticals and ^{111}In Immuno-Single Photon Emission Computed Tomography Imaging. *Bioconjugate Chem.* **2017**, *28*, 2145−2159.
(42) Wang, X.; Jaraquemada-Peláez, M.; de, G.; Rodríguez-Rodríguez, C.; Cao, Y.; Buchwalder, C.; Choudhary, N.; Jermilova, U.; Ramogida, C. F.; Saatchi, K.; Häfeli, U. O.; et al. H_4Octox: Versatile Bimodal Octadentate Acyclic Chelating Ligand for Medicinal Inorganic Chemistry. *J. Am. Chem. Soc.* **2018**, *140*, 15487−15500.
(43) Price, E. W.; Zeglis, B. M.; Cawthray, J. F.; Ramogida, C. F.; Ramos, N.; Lewis, J. S.; Adam, M. J.; Orvig, C. H_4Octapa-Trastuzumab: Versatile Acyclic Chelate System for ^{111}In and ^{177}Lu Imaging and Therapy. *J. Am. Chem. Soc.* **2013**, *135*, 12707−12721.
(44) Safarzadeh, L.; Ghannadi-Maragheh, M.; Anvari, A.; Aghamiri, S. M. R.; Shirvani-Arani, S.; Bahrami-Samani, A. Production, Radiolabeling and Biodistribution Studies of ^{175}Yb-DOTMP as Bone Pain Palliation. *Iran. J. Pharm. Sci.* **2012**, *8*, 135−141.
(45) Salek, N.; Vosoghi, S.; Arani, S. S.; Samani, A. B.; Mehrabi, M.; Maraghe, M. G. Preparation and Dosimetry Evaluation of a Carrier-Free ^{90}Y Labeled DOTMP as a Promising Agent for Bone Marrow Ablation. *Curr. Radiopharm.* **2018**, *11*, 116−122.
(46) Yousefnia, H.; Zolghadri, S. Human Absorbed Dose Estimation of a New In-111 Imaging Agent Based on Rat Data. *Int. J. Phys. Math. Sci.* **2015**, *9*, 627−631.
(47) Zolghadri, S.; Yousefnia, H.; Jalilian, A. R.; Ghannadi-Maragheh, M. Production, Biodistribution Assessment and Dosimetric Evaluation of ^{177}Lu-TTHMP as an Agent for Bone Pain Palliation. *Asia Ocean. J. Nucl. Med. Biol.* **2015**, *3*, 35−42.
(48) Comba, P.; Jermilova, U.; Orvig, C.; Patrick, B. O.; Ramogida, C. F.; Rück, K.; Schneider, C.; Starke, M. Octadentate Picolinic Acid-Based Bispidine Ligand for Radiometal Ions. *Chem. - Eur. J.* **2017**, *23*, 15945−15956.
(49) Boros, E.; Ferreira, C. L.; Cawthray, J. F.; Price, E. W.; Patrick, B. O.; Wester, D. W.; Adam, M. J.; Orvig, C. Acyclic Chelate with Ideal Properties for ^{68}Ga PET Imaging Agent Elaboration. *J. Am. Chem. Soc.* **2010**, *132*, 15726−15733.
(50) Cotton, S. A. *Lanthanide and Actinide Chemistry*; John Wiley & Sons: West Sussex, 2006.
(51) Paúrová, M.; Havlíčková, J.; Pospíšilová, A.; Vetrík, M.; Císařová, I.; Stephan, H.; Pietzsch, H.-J.; Hrubý, M.; Hermann, P.; Kotek, J. Bifunctional Cyclam-Based Ligands with Phosphorus Acid Pendant Moieties for Radiocopper Separation: Thermodynamic and Kinetic Studies. *Chem. - Eur. J.* **2015**, *21*, 4671−4687.
(52) Baranyai, Z.; Reich, D.; Vágner, A.; Weineisen, M.; Tóth, I.; Wester, H.-J.; Notni, J. A Shortcut to High-Affinity Ga-68 and Cu-64 Radiopharmaceuticals: One-Pot Click Chemistry Trimerisation on the TRAP Platform. *Dalton Trans.* **2015**, *44*, 11137−11146.
(53) Dash, A.; Pillai, M. R. A.; Knapp, F. F. Production of ^{177}Lu for Targeted Radionuclide Therapy: Available Options. *Nucl. Med. Mol. Imaging* **2015**, *49*, 85−107.
(54) Banerjee, S.; Pillai, M. R. A.; Knapp, F. F. Lutetium-177 Therapeutic Radiopharmaceuticals: Linking Chemistry, Radiochemistry, and Practical Applications. *Chem. Rev.* **2015**, *115*, 2934−2974.
(55) Zeng, X.; Coquière, D.; Alenda, A.; Garrier, E.; Prangé, T.; Li, Y.; Reinaud, O.; Jabin, I. Efficient Synthesis of Calix[6]Tmpa: A New Calix[6]Azacryptand with Unique Conformational and Host−Guest Properties. *Chem. - Eur. J.* **2006**, *12*, 6393−6402.
(56) Gran, G. Determination of the Equivalence Point in Potentiometric Titrations. Part II. *Analyst* **1952**, *77*, 661.
(57) Frisch, M. J.; Trucks, G. W.; Schlegel, H. B.; Scuseria, G. E.; Robb, M. A.; Cheeseman, J. R.; Scalmani, G.; Barone, V.; Petersson,

https://dx.doi.org/10.1021/acs.inorgchem.0c00671
Inorg. Chem. XXXX, XXX, XXX−XXX

G. A.; Nakatsuji, H.; Li, X.; Caricato, M.; Marenich, A. V.; Bloino, J.; Janesko, B. G.; Gomperts, R.; Mennucci, B.; Hratchian, H. P.; Ortiz, J. V.; Izmaylov, A. F.; Sonnenberg, J. L.; Williams-Young, D.; Ding, F.; Lipparini, F.; Egidi, F.; Goings, J.; Peng, B.; Petrone, A.; Henderson, T.; Ranasinghe, D.; Zakrzewski, V. G.; Gao, J.; Rega, N.; Zheng, G.; Liang, W.; Hada, M.; Ehara, M.; Toyota, K.; Fukuda, R.; Hasegawa, J.; Ishida, M.; Nakajima, T.; Honda, Y.; Kitao, O.; Nakai, H.; Vreven, T.; Throssell, K.; Montgomery, J. A., Jr.; Peralta, J. E.; Ogliaro, F.; Bearpark, M. J.; Heyd, J. J.; Brothers, E. N.; Kudin, K. N.; Staroverov, V. N.; Keith, T. A.; Kobayashi, R.; Normand, J.; Raghavachari, K.; Rendell, A. P.; Burant, J. C.; Iyengar, S. S.; Tomasi, J.; Cossi, M.; Millam, J. M.; Klene, M.; Adamo, C.; Cammi, R.; Ochterski, J. W.; Martin, R. L.; Morokuma, K.; Farkas, O.; Foresman, J. B.; Fox, D. J. *Gaussian 16*, Revision C.01; Gaussian, Inc.: Wallingford, CT, 2016.

(58) Tao, T.; Perdew, J. P.; Staroverov, V. N.; Scuseria, G. E. Climbing the Density Functional Ladder: Nonemperical Meta-Generalized Gradient Approximation Designed for Molecules and Solids. *Phys. Rev. Lett.* **2003**, *91*, 146401.

(59) Schäfer, A.; Huber, C.; Ahlrichs, R. Fully Optimized Contracted Gaussian Basis Sets of Triple Zeta Valence Quality for Atoms Li to Kr. *J. Chem. Phys.* **1994**, *100*, 5829−5835.

(60) Dolg, M.; Wedig, U.; Stoll, H.; Preuss, H. Energy-adjusted Ab Initio Pseudopotentials for the First Row Transition Elements. *J. Chem. Phys.* **1987**, *86*, 866−872.

(61) Dolg, M.; Stoll, H.; Preuss, H. Energy-adjusted Ab Initio Pseudopotentials for the Rare Earth Elements. *J. Chem. Phys.* **1989**, *90*, 1730−1734.

https://dx.doi.org/10.1021/acs.inorgchem.0c00671
Inorg. Chem. XXXX, XXX, XXX−XXX